Asian Journal of Chemistry; Vol. 37, No. 6 (2025), 1399-1414

ASIAN JOURNAL OF CHEMISTRY

https://doi.org/10.14233/ajchem.2025.33802

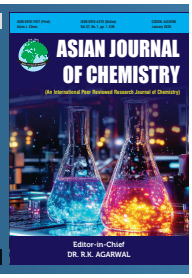

Synthesis, Electronic, Spectroscopic and Molecular Structure Investigation on Anticancer Drug Spirooxindole-Chromene Derivative

P. SWARNAMUGHI[1,*], M. KUMAR[1], P. MANIKANDAN[1], S. CHITHRA[1], MOHD ASIF[2], MALIK NASIBULLAH[2,*] and A. PRABAHARAN[3]

[1]Department of Physics, Arignar Anna Government Arts College, Cheyyar-604407, India
[2]Medicinal Chemistry Laboratory-ICEIR, Department of Chemistry, Integral University, Lucknow-226026, India
[3]Department of Physics, Vel Tech Rangarajan Dr Sagunthala R&D Institute of Science and Technology, Avadi, Chennai-600062, India

*Corresponding authors: E-mail: saroswarna96@gmail.com; malik@iul.ac.in

Received: 3 April 2025; *Accepted*: 8 May 2025; *Published online*: 27 May 2025; AJC-22014

This work explores carbon-carbon bond formation *via* Michael addition in synthesizing a novel spirooxindole-chromene derivative (**4**) using click chemistry, examining its quantum parameters and potential anticancer effects. Spectroscopic methods, including UV-800, FT-IR and NMR, were used alongside quantum calculations (IEFPCM model) to validate the molecular structure. The compound was optimized in the gas phase with a 6-311++G(d,p) basis set and VEDA was employed for vibrational assignments. Drug-likeness properties were assessed using the ADMET online tool. *In vitro* studies with sixty human cancer cell lines indicated that compound **4** showed 17.88% resistance against UO-31 renal cancer cells at 10^{-5} M. Virtual screening identified active sites related to anticancer proteins 4DRI, 6CZ4 and 8BR9, with binding energies of -7.76, -7.3 and -6.59 kcal/mol, respectively. Ramachandran plots indicated favourable conformations for docking, with blue areas representing optimal binding positions. Ultimately, compound **4** may be enhanced for anticancer efficacy through elimination reactions at its primary amine position on the pyrano ring.

Keywords: Synthesis, Indole derivative, Density functional theory, Anticancer activity, Molecular docking.

INTRODUCTION

Indole-containing heterocyclic compounds have been extracted from natural genesis and as well as synthesized making use of an assortment of approaches [1]. Indeed, such yielded and extracted compounds have proved to have an important effect on reducing the unregulated growth of cells in living organisms, which originate cancer. Nowadays, surviving cancer disease has become an exhausting strategy deploying several medications, although chemotherapy is regarded as the more effective option [2]. As a result, despite the FDA and NCI-approved indole-containing drugs, there is a need for new drug discoveries, such as those that could be less toxic and more effective at hindering human cancer cells.

Spirooxindole is a spiro molecule containing atleast two molecular rings sharing a common atom, playing a significant role in synthetic and medicinal chemistry. Significant efforts have been made to utilize this spirocyclic motif as a fundamental structure in the synthesis of new drug candidates, many of which demonstrate promising biological and pharmacological profiles [3-6]. Recently, Asif *et al.* [7-11] published work related to the synthesis of spirooxindole derivatives utilizing multiple chemical techniques and they also proved the anticancer efficacy of some spirooxindoles. Moreover, the 4*H*-pyran framework and its derivatives constitute the privileged structures of various oxygen containing heterocyclic organic compounds [12,13]. Thus, the hybridization of spirooxindole and 4H-pyran rings together have the potential to produce novel therapeutic effects or greatly enhance existing biological activity.

Several studies has shown that computer-aided drug design approaches are crucial to the development of new drugs [14,15]. As a possible computational approach, density functional theory (DFT) evaluates bonding, structural characteristics and vibrational modes of organic molecules. In this work, we are interested to synthesize indole-containing small spiro-drug-like molecule using organic building blocks like reactive molecules,

namely dioxindole, malononitrile, 5,5-dimethylcyclohexane-1, 3-dione and triethylamine (Et_3N) as Lewis base, which were used for heterogeneous catalysis to form spiro-oxindole-chromene derivatives using one-pot click chemistry under Knoevenagel condensation and Michael addition reactions (Fig. 1). The pharmacological characteristics of the substance under investigation are validated by the ADME drug-likeness experiments. The synthesized compounds are also evaluated for their *in vitro* anticancer activity against 60 human cancer cell lines.

EXPERIMENTAL

The chemicals and solvents were procured from various chemical commercial suppliers like Aldrich, Merck and TCI Chemicals and were used as received. All the solvents used in the present study were dried by known purification technique. Using the open capillary tube procedure and a Griffin Equipment IA 9100 MK-Digital incorrect point of melting detector, the melting point of the material was ascertained. Agilent Cary 630 Fourier transform-infrared spectroscopy (4000-450 cm^{-1}) was used to collect the infrared spectra. FT-Raman were recorded with BRUKER RFS 27 MultiRAM FT Raman Spectrometer. ^1H NMR spectra were obtained with a Brucker Advance-400 MHz in DMSO-d_6 solvent using trimethylsilane as an internal reference . The ^{13}C NMR spectra were obtained with BAVLL-100 MHz (Brucker, Switzerland) using DMSO-d_6 solvent.

Synthesis of spirooxindole-chromene derivatives: Three reactive molecules, namely 5,5-dimethylcyclohexan-1,3-dione, dioxindole and malononitrile, were utilized in a similar equivalent for the synthesis of spirooxindole-chromene derivative (2-amino-7,7-dimethyl-2′,5-dioxo-4a,5,6,7,8,8a-hexahydro-spiro[chromene-4,3′-indoline]-3-carbonitrile) under the click chemistry, owing to Lewis base being used as catalyst in a single pot reaction system (**Scheme-I**). The thin-layer chromatography method was followed to check the reaction progress and column chromatography was applied to purify the product before extraction with *n*-hexane and ethyl acetate combined, a pure compound in white was obtained [16].

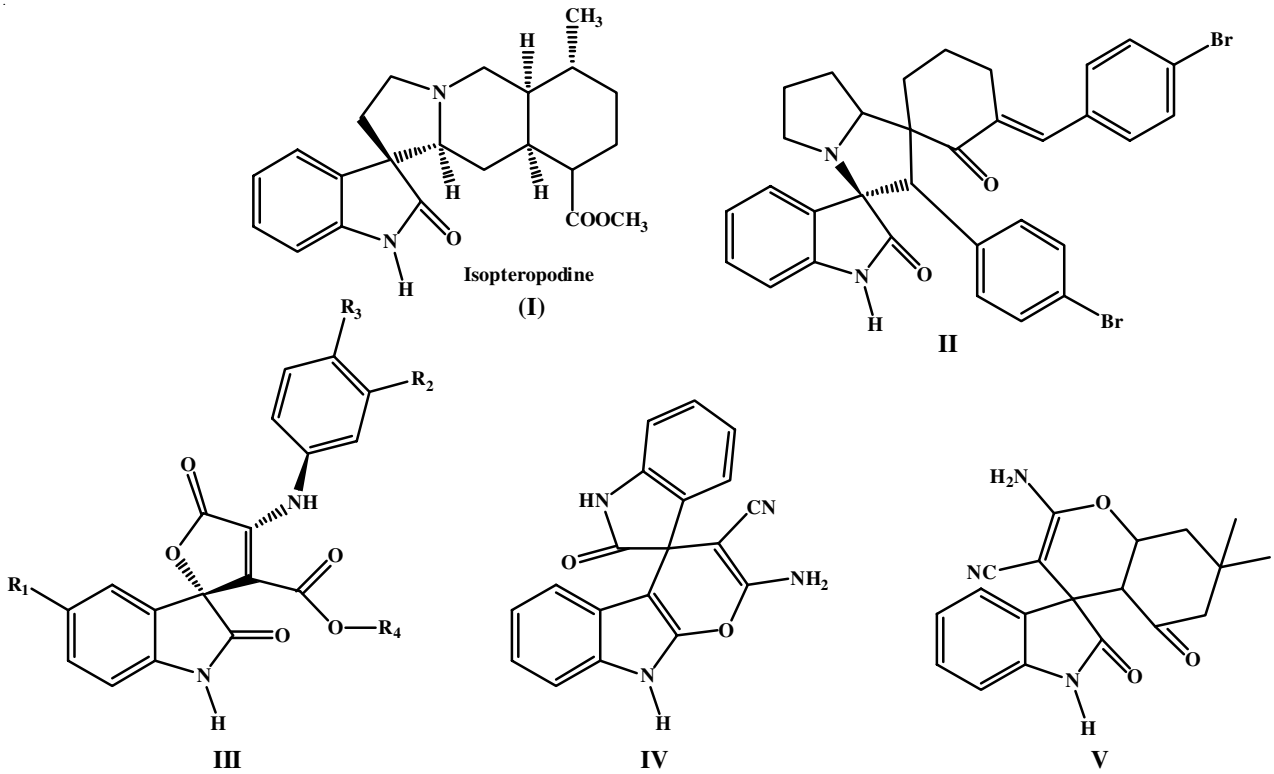

Fig. 1. Spiroixindole-containing anticancer agents (**I-IV**) and proposed synthesized active molecule (**V**)

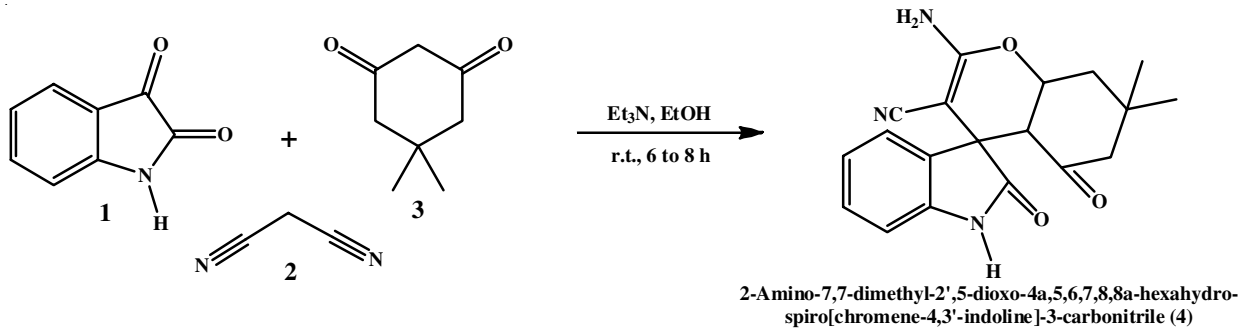

Scheme-I: Proposed reaction for the synthesis of spirooxindole-chromene derivative (**4**)

Quantum chemical computational details: A Gaussian 16 with 6-311++G(d,p) basis-set and Gauss view 6 is employed for computational calculations [17,18]. Chemcraft 1.8 software was used to optimize the structure of compound **4** [19]. The computational analysis was performed to calculate the optimized geometrical parameters, energy, fundamental vibrational frequencies, IR intensity, Raman intensity, FMOs analysis, NBO analysis, NMR analysis, dipole moments and other parameters. The wavenumbers have been manipulated with a factor of 0.961 as in this work, the wavenumbers are scaled using a particular factor 0.961 [20]. Using the combined output of VEDA 4 and Gauss-View 6 software, the vibrational wave number assignments were noted [21]. The HOMO-LUMO, NLO and MEP have been carried out. To understand the relationships within the orbital, the NBO computations have been assessed. The dual descriptor and the same set of bases were employed for the computation to calculate the Fukui function. Multiwfn 3.8 was used to estimate topological parameters, including LOL, ELF [22]. Atomistica online tool was used to draw the RDG scatter plot [23,24]. To find the drug-likeness characteristics, the ADME analysis was performed on the synthesized compounds using the SWISS-ADME web tool [25]. Autodock software was used to analyze and visualize molecular docking interactions [26]. Using Discovery Studio Visualizer, the resulting docked conformations were also interpreted [27].

RESULTS AND DISCUSSION

The synthesis of novel spirooxindole-chromene compound (**4**) was carried out with Et_3N as catalyst which underwent Knoevenegel and Michael addition reactions (**Scheme-I**). In the synthesis, three reactive reactant species, namely, 5,5-dioxindole (**1**), dimethylcyclohexan-1,3-dione (**3**) and highly reactive methylene compound (**2**) were used. Eventually, dioxindole and malononitrile were reacted using a Et_3N Lewis base catalyst for 15 to 21 min, resulting in α,β-unsaturated molecule, also known as isatin-malononitrile intermediate **3**. Furthermore, (5-dimethyl cyclohexane-1,3-dione) showed two resonating strictures, 3-hydroxy-5,5-dimethyl cyclohex-2-en-1-one, which reacts with α,β-unsaturated intermediate under the Michael addition process, resulting in another unstable intermediate. It was cyclized and tautomerized, yielding a stable spirooxindole-chromene compound(**4**) (**Scheme-II**).

Molecular geometry: The bond angle and bond length enhance the geometric arrangement of the computed compound **4**. As illustrated in Fig. 2, an optimized structure is achieved using the DFT method in gas phase [28]. The values of the geo-

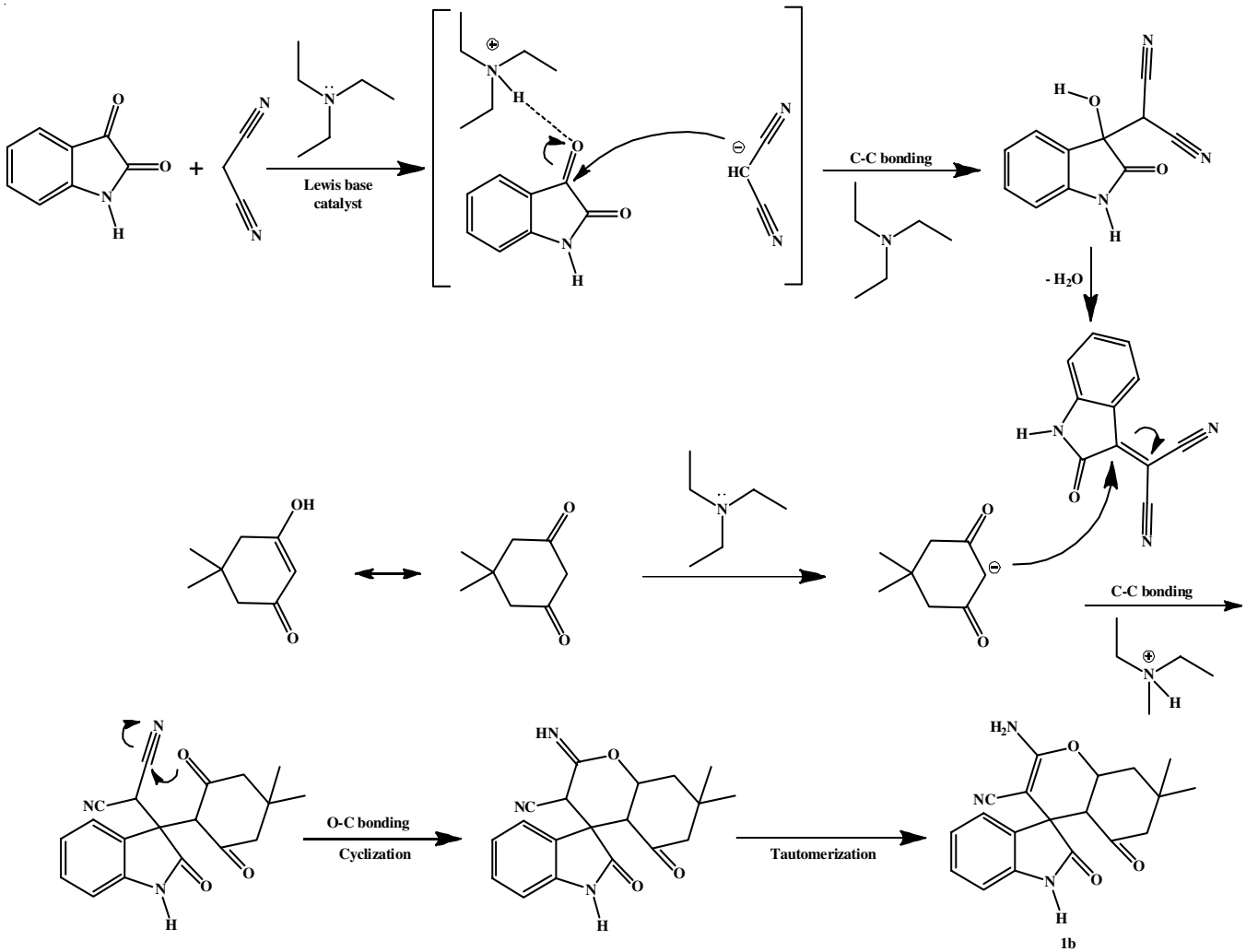

Scheme-II: Plausible reaction strategy for the synthesis of spirooxindole-chromene

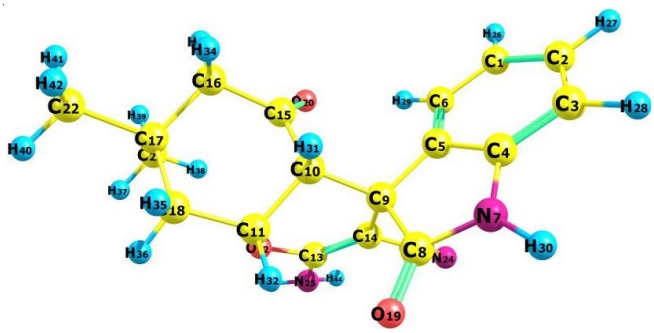

Fig. 2. Optimized geometric structure with atom numbering of compound **4**

metrical requirements listed above are summarized in Table-1. Compound **4** has 47 bond length and 86 bond angle. There are twenty (CC), sixteen (CH), three (NH), four (CN) and four (CO). The increased bond lengths of the atom are associated with carbon-carbon connections at (C8-C9, C9-C10, C16-C17, C10-C11), measuring (1.578 Å, 1.56 Å, 1.559 Å, 1.546 Å), resulting from repulsion among the homonuclear atoms. In contrast, the interactions at (N25-H43, N25-H44, N7-H30, C6-H29) exhibit calculated lengths of (1.007 Å, 1.008 Å, 1.01 Å, 1.08 Å), is due to the attraction between heteronuclear atoms. The maximum bond angle occured at (C14-C23-N24), (C6-

TABLE-1
GEOMETRICAL PARAMETERS OF COMPOUND **4**: BOND LENGTH (Å) AND BOND ANGLE (º)

Bond length (Å)	B3LYP/6-311++G(d,p)	Bond angle (º)	B3LYP/6-311++G(d,p)	Bond angle (º)	B3LYP/6-311++G(d,p)
C1-C2	1.393	C2-C1-C6	120.8	C11-C18-C17	117
C1-C6	1.399	C2-C1-H26	119.8	C11-C18-H35	105.8
C1-H26	1.084	C1-C2-C3	120.7	C11-C18-H36	108.5
C2-C3	1.397	C1-C2-H27	119.9	O12-C13-C14	123.9
C2-H27	1.084	C6-C1-H26	119.4	O12-C13-N25	111.3
C3-C4	1.387	C1-C6-C5	119.3	C14-C13-N25	124.9
C3-H28	1.084	C1-C6-CH29	120.5	C13-C14-C23	117.7
C4-C5	1.401	C3-C2-H27	119.3	C13-N25-H43	116.9
C4-N7	1.403	C2-C3-C4	117.6	C13-N25-H44	118.4
C5-C6	1.388	C2-C3-H28	121.1	C14-C23-N24	177.6
C5-C9	1.531	C4-C3-H28	121.3	C16-C15-O20	122.6
C6-H29	1.08	C3-C4-C5	122.7	C15-C16-C17	111.2
N7-C8	1.369	C3-C4-N7	127.6	C15-C16-H33	108.7
N7-H30	1.01	C5-C4-N7	109.7	C15-C16-H34	108.9
C8-C9	1.578	C4-C5-C6	118.9	C17-C16-H33	110.6
C8-O19	1.214	C4-C5-C9	109.1	C17-C16-H34	109
C9-C10	1.56	C4-N7-C8	112.5	C16-C17-C18	108.9
C9-C14	1.518	C4-N7-H30	125.2	C16-C17-C21	109.8
C10-C11	1.546	C6-C5-C9	131.9	C16-C17-C22	108.9
C10-C15	1.534	C5-C6-H29	120.2	H33-C16-C34	108.4
C10-H31	1.095	C5-C9-C8	101.1	C18-C17-C21	111.8
C11-O12	1.453	C5-C9-C10	115	C18-C17-C22	108.8
C11-C18	1.526	C5-C9-C14	114.8	C17-C18-H35	108.8
C11-H32	1.091	C8-N7-H30	121.6	C17-C18-H36	109.9
O12-C113	1.347	N7-C8-C9	107.3	C21-C17-C22	108.6
C13-C14	1.37	N7-C8-O19	125.6	C17-C21-H37	110.3
C13-N25	1.362	C9-C8-O19	127.1	C17-C21-H38	112.5
C14-C23	1.412	C8-C9-C10	105.6	C17-C21-H39	110.2
C15-C16	1.517	C8-C9-C14	110.5	C17-C22-H40	110.8
C15-O20	1.209	C10-C9-C14	109.2	C17-C22-H41	110.9
C16-C17	1.559	C9-C10-C11	109.6	C17-C22-H42	111.5
C16-H33	1.092	C9-C10-C15	118.4	H35-C18-H36	106.3
C16-H34	1.097	9-C14-H31	108.6	H37-C21-H38	107.8
C17-C18	1.55	C9-C14-C13	121.9	H37-C21-H39	107.8
C17-C21	1.542	C9-C14-C23	120.3	H39-C21-H39	108
C17-C22	1.539	C11-C10-C15	106.2	H40-C22-H41	107.7
C18-H35	1.096	C11-C10-H31	106.7	H40-C22-H42	107.9
C18-H36	1.094	C10-C11-O12	109.2	H41-C22-H42	108
C21-H37	1.094	C10-C11-C18	113.4	H43-N25-H44	117.5
C21-H38	1.09	C10-C11-H32	108.9		
C21-H39	1.094	C15-C10-H31	106.8		
C22-H40	1.094	C10-C15-C16	112.6		
C22-H41	1.094	C10-C15-O20	124.6		
C22-H42	1.094	O12-C11-C18	108.6		
C23-N24	1.161	O12-C11-H32	106.7		
N25-H43	1.007	C11-O12-C13	117.5		
N25-H44	1.008	C18-C11-H32	109.9		

C5-C9), (C3-C4-N7), (N7-C8-O19) have angles (1.776º, 131.9º, 127.6º, 125.6º), minimum bond angles (C5-C9-C8), (C8-C9-C10), (H35-C18-H36), (H40-C22-H41) occurs at (101.1, 105.6, 106.3, 107.7) relatively.

Spectroscopic vibrations: Several molecular functional groups are recognized. Both computational and experimental DFT/basis levels in the gas phase were used to obtain the FT-IR and FT-Raman spectra. Part of the C1point set is comprised of the chemical structure of compound **4**, which is assumed to include 44 atoms and 126 normal vibration modes. The vibrational modes are subjected to formula 3n-6 to yield the title molecule. The unscaled wavenumbers are then reduced to the experimental wavenumbers using the scaling function 0.961 [29,30]. Table-2 provided a summary of the IR frequencies, Raman intensities, prompted wavenumbers and potential energy distribution effects. Figs. 3 and 4 display the simulated spectra.

TABLE-2
VIBRATIONAL SPECTRAL ANALYSIS USING DFT METHOD, BASIS SET WITH PED ASSIGNMENTS OF COMPOUND **4**

Modes	Experimental wavenumbers (cm^{-1})		Theoretical wavenumber (cm^{-1})		IR[c] intensity		[d]Raman activity		[a]PED assignments
	FT-IR	FT-Raman	Unscaled	Scaled[b]	IR	IA	RR	RA	
126	–	–	3710	3565	55	10	50	17	ν NH 100
125	–	–	3625	3483	52	10	209	70	ν NH 100
124	3377	–	3590	3450	74	14	150	50	ν NH 100
123	3141	–	3233	3107	2	0	61	21	ν CH 98
122	–	–	3191	3067	17	3	280	94	ν CH 98
121	–	3058	3180	3056	13	2	117	39	ν CH 94
120	–	–	3168	3045	2	0	63	21	ν CH 99
119	–	–	3126	3004	17	3	43	15	ν CH 87
118	–	–	3098	2977	25	5	105	35	ν CH 94
117	–	–	3092	2972	7	1	63	21	ν CH 99
116	–	–	3088	2968	38	7	113	38	ν CH 94
115	–	–	3084	2964	23	4	54	18	ν CH 97
114	–	2959	3082	2962	13	2	36	12	ν CH 96
113	2959	–	3067	2948	10	2	56	19	ν CH 96
112	2926	2929	3042	2923	17	3	124	41	ν CH 88
111	–	–	3031	2913	22	4	298	100	ν CH 77
110	2885	–	3024	2906	29	5	51	17	ν CH 69
109	–	–	3020	2902	11	2	29	10	ν CH 66
108	–2657	2887	3016	2899	17	3	50	17	ν CH 90
107	2192	2192	2288	2199	117	22	251	84	ν NC 88 + ν CC 12
106	1722	–	1793	1723	102	19	9	3	ν OC 89
105	1683	–	1781	1712	540	100	15	5	ν OC 81
104	1655	1655	1661	1596	439	81	36	12	ν CC 26 + ν NC 16 + β HNH 41
103	1604	1602	1658	1593	86	16	20	7	ν CC 43
102	–	–	1632	1568	10	2	29	10	ν CC 56 + β CCC 10
101	–	–	1612	1549	191	35	22	7	ν CC 31 + β HNC 13 + β HNH 37
100	1471	1470	1512	1453	9	2	1	0	β HCC 52
99	–	–	1512	1453	13	2	1	0	β HCH 70
98	–	–	1507	1449	3	1	11	4	β HCH 72
97	–	–	1501	1442	71	13	14	5	ν CC 16 + ν 11 + β HCC 30
96	–	–	1497	1438	7	1	1	0	β HCH 53
95	–	–	1488	1430	2	0	10	3	β HCH 77
94	–	–	1476	1419	3	1	4	1	β HCH 51
93	–	1404	1470	1413	6	1	4	1	β HCH 83
92	1391	–	1445	1389	67	12	1	0	ν NC 19 + ν OC 16 + β HCO 31
91	–	–	1429	1373	12	2	0	0	β HCH 61
90	–	–	1420	1364	25	5	24	8	ν NC 13 + β HNC 32 + β HCC 19
89	–	–	1406	1351	8	1	1	0	τ HCOC 11 + β HCH 64
88	1348	–	1402	1347	4	1	3	1	β HCC 16 + τ 35
87	1325	–	1384	1330	48	9	4	1	β HCO 25 + τ HCCC 14
86	–	–	1368	1315	117	22	2	1	β HCO 24 + τ HCCC 14
85	1297	–	1345	1293	15	3	4	1	ν CC 13
84	–	–	1341	1289	17	3	1	0	ν CC 10 + β HCC 12 + τ HCCC 10
83	1261	–	1317	1265	5	1	10	3	β HCC 23
82	–	–	1307	1256	16	3	1	0	τ HCCC 41
81	–	–	1304	1254	20	4	12	4	ν CC 24 + β HCC 16
80	1222	1224	1273	1223	14	3	11	4	ν CC (18) + β HCC (41)
79	–	–	1269	1219	54	10	4	1	ν NC 30 + β HCC 12

78	–	–	1258	1209	8	1	4	1	ν CC 21
77	–	–	1238	1189	60	11	11	4	τ HCCC 25
76	–	–	1232	1184	17	3	16	5	ν CC 16 + β CCC 10
75	–	–	1221	1173	58	11	14	5	β HCC 20
74	1165	–	1209	1162	15	3	11	4	ν NC 10
73	–	–	1197	1150	20	4	4	1	ν CC 12 + τ HCCC 20
72	–	–	1186	1140	14	3	4	1	ν CC 11 + β HCC 40
71	–	–	1179	1133	39	7	10	3	β HCC 13
70	–	–	1171	1125	1	0	21	7	β HCC 20
69	1089	1071	1124	1080	17	3	2	1	ν CC 24
68	1054	–	1109	1066	115	21	4	1	ν OC 18 + β HNC 16
67	–	–	1088	1046	13	2	6	2	ν CC 15 + τ HCCC 13
66	–	–	1082	1040	10	2	2	1	ν CC 18
65	–	–	1062	1021	54	10	6	2	ν CC 10 + ν CC 38 + β HCC 11 + β HCC 17
64	–	–	1048	1007	4	1	36	12	ν CC 63 + β HCC 12
63	986	–	1036	996	1	0	1	0	τ HCCC 34 + τ CCCC 20
62	–	–	1015	975	9	2	3	1	ν CC 15
61	–	–	998	959	1	0	0	0	τ HCCC 86
60	–	–	991	952	7	1	3	1	τ HCCC 71
59	–	–	966	929	6	1	0	0	τ HCCC 73
58	924	–	964	926	5	1	1	0	ν OC 15
57	–	–	951	913	7	1	4	1	ν CC 22 + τ HCCC 25
56	902	–	938	901	17	3	3	1	ν CC 19
55	–	–	926	890	3	1	2	1	τ HCCC 13 + τ HCCC 75
54	–	–	922	886	1	0	4	1	ω CCOC 12
53	873	–	905	870	5	1	3	1	ν CC 11
52	–	–	891	856	3	0	4	1	β CCC 17
51	–	–	873	839	2	0	2	1	τ HCCC 95
50	–	–	869	835	0	0	0	0	τ HCCC 84
49	–	–	829	797	11	2	1	0	ν OC 11
48	–	–	811	779	3	0	1	0	ω OCNC 16
47	745	–	773	743	2	0	0	0	τ CCCC 20
46	–	–	763	733	46	9	1	0	τ HCCC45
45	–	–	754	724	18	3	1	0	τ HCCC10 + ω OCNC 11
44	–	688	720	692	8	1	3	1	ω NCOC 44
43	678	–	697	670	2	0	1	0	ω OCNC 14 + ω NCOC 13
42	–	–	690	663	16	3	18	6	β CCC 10 + β CNC 18
41	–	–	668	642	4	1	11	4	β CCC 12
40	–	–	659	633	5	1	6	2	β CCC 11
39	614	625	650	625	1	0	3	1	β CCC 22
38	–	–	627	602	18	3	3	1	β OCN 19 + β NCC 11
37	–	–	605	581	9	2	4	1	ω OCCC 28
36	557	–	577	555	4	1	6	2	ν OC10 + β NCC 10
35	–	–	568	545	3	1	1	0	τ CCCC 40
34	–	–	561	539	7	1	0	0	τ NCCC 45 + ω CCCC 13
33	–	518	544	522	61	11	2	1	β OCC 14 + τ HNCC 19
32	–	490	508	488	29	5	4	1	τ HNCC 30
31	–	–	492	472	4	1	5	2	β OCC 14
30	–	–	487	468	9	2	7	2	β CCC 11 + β CNC 10
29	–	–	464	446	6	1	1	0	τ HNCC25 + ω NCCC 15
28	–	–	446	429	34	6	1	0	β NCO 11 + τ HNCC
27	–	–	431	414	2	0	1	0	ω CCCC 17
26	–	–	426	410	18	3	1	0	τ HNCC 33
25	–	–	399	383	1	0	0	0	β CCC 39
24	–	–	376	361	0	0	2	1	ω CCCC 46
23	–	–	373	358	1	0	2	1	β NCC 10 + β CCC 10
22	–	–	359	345	4	1	2	1	β NCC 13 + β CCC 14
21	–	–	331	318	195	36	1	0	τ HNCC 75
20	–	–	319	306	9	2	2	1	τ CCCC 13
19	–	–	316	304	6	1	2	1	β CCC 10 + β CNC 18
18	–	–	302	291	10	2	0	0	τ NCCC 62
17	–	–	281	270	4	1	1	0	τ HCCC 14

16	–	–	269	258	1	0	1	0	β CCC 14
15	–	233	250	240	0	0	1	0	τ HCCC 15 + ω CCCC 14
14	–	–	235	226	1	0	2	1	τ HCCC 10
13	–	–	228	219	3	1	1	0	β CCC 12
12	–	–	210	202	1	0	2	1	τ CCOC 10 + τ COCC 23 + ω CCCC 10
11	–	196	206	198	1	0	3	1	β CNC 17
10	–	–	197	189	1	0	1	0	τ CCOC 18 + τ COCC 11
9	–	146	158	152	2	0	0	0	τ CNCC 27 + ω CCCC 57
8	–	–	139	133	5	1	1	0	β NCC 13 + β CCC 25 + τ CNCC 13 + ω OCCC 11
7	–	116	113	109	3	1	1	0	β NCC 15 + β CCC 19 + τ CNCC 19
6	–	–	95	91	3	1	1	0	τ CCCC 33
5	–	77	88	84	0	0	1	0	τ CCCC 33
4	–	–	72	69	0	0	3	1	β CCO 11 + τ CCCC 10 + τ COCC 11
3	–	–	65	63	1	0	4	1	τ CCCC 27 + ω CCCC 11 + ω CCCC 10
2	–	–	45	43	2	0	5	2	β CCC 23 + τ CCCC 29 + ω CCCC 12
1	–	–	42	40	3	1	1	0	β CCC 23 + τ CCCC10 + τOCCC 23 + τCOCC 12

[a]Scaling factor: 0.961, basis set B3LYP/6-311++G(d,p); [b]Relative IR absorption normality intensities with highest peak absorption equal to 100; [c]Relative Raman intensities normalized to 100; [d]Stretching-ν, bending-β, torsion-τ.

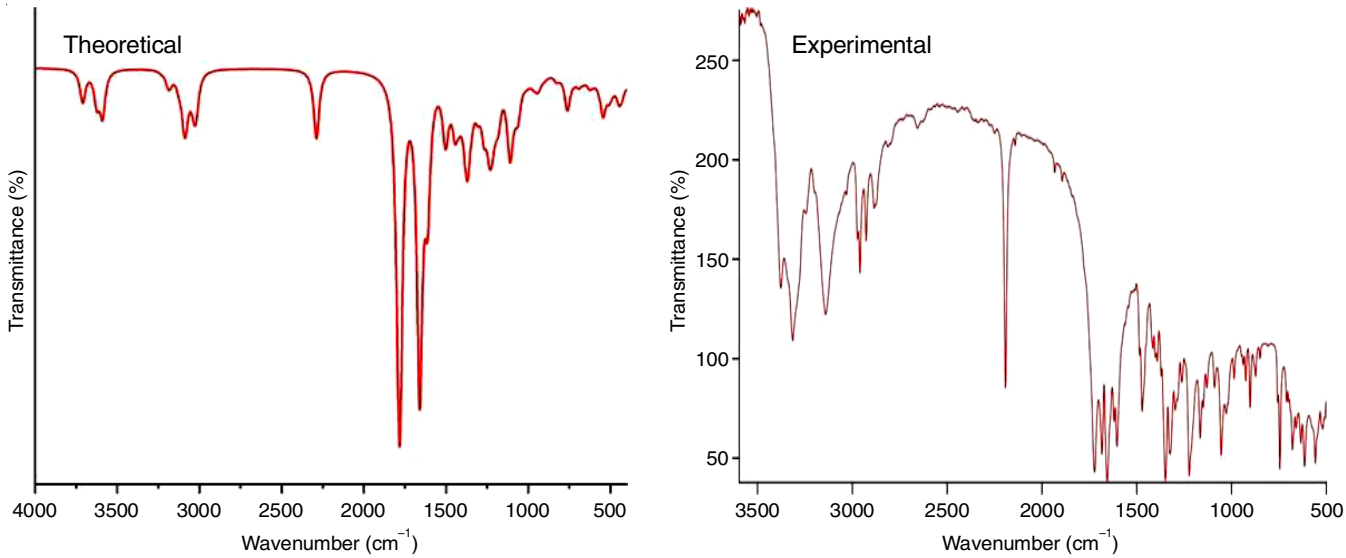

Fig. 3. Comparative IR spectra of compound **4**

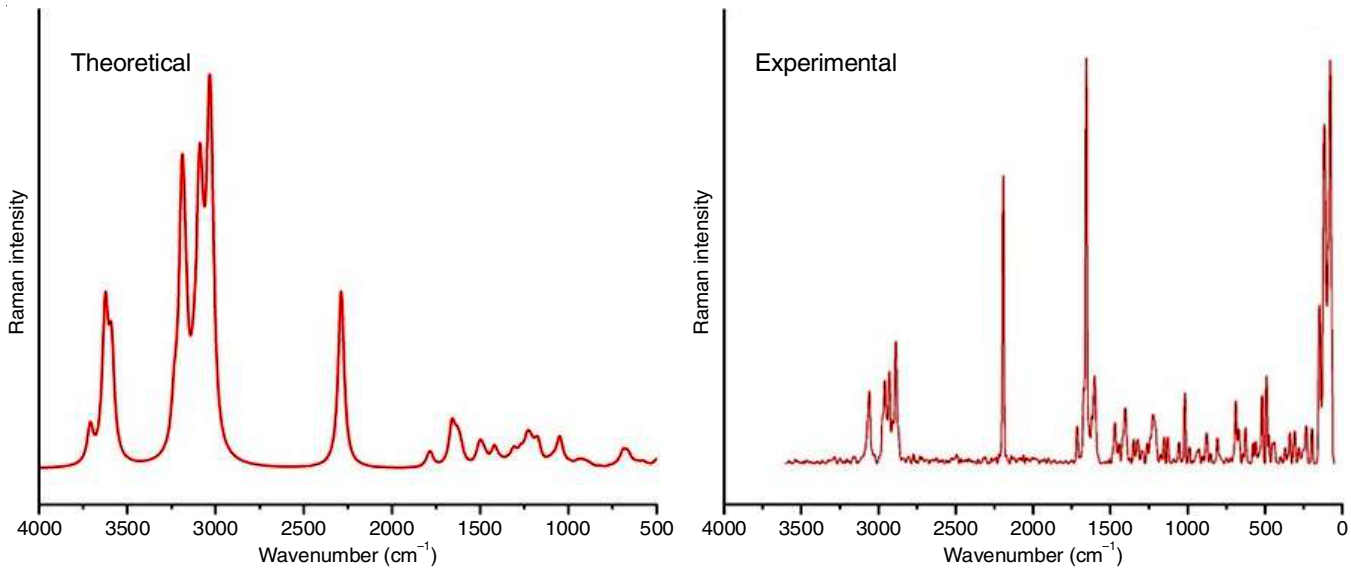

Fig. 4. Comparative Raman spectra of compound **4**

C-H vibration: Some peaks in the 3100-3000 cm^{-1} range is demonstrated by heteroatomic molecules in ν(CH) [31]. PED-contributed theoretical C-H vibrations of stretching were obtained at 3107(99%)-2899(66%) cm^{-1}. Experimental C-H vibrations were identified as the source of frequencies observed at 3141-2657 cm^{-1} for IR and 3058-2887 cm^{-1} for Raman.

N-H vibration: Within the range of 3500-3300 cm^{-1}, NH stretching was estimated [32]. Experimentally observed vibrations for FT-IR were 3377 (100%) cm^{-1}, while the theoretically scaled wavenumbers were 3565, 3483 and 3450 cm^{-1} with PED contributions.

Carbonyl group vibrations: The C-O vibrations stretching mode centers was observed around 1850-1550 cm^{-1} [33]. Theoretically, the stretching vibrations of PED range from 1781 cm^{-1} (89%) to 1723 cm^{-1} (81%), but empirical observations for compound **4** in FT-IR spectra indicate a range of 1722-1683 cm^{-1}.

C-C vibration: The expected range for a phenyl vibration of stretching is 1600-1100 cm^{-1} [34]. FT-infrared, FT-Raman and hypothetically observed at 1604, 1297, 1089 cm^{-1} and 1602-1071 cm^{-1}, respectively, consisting of 1593 (43%), 1293 (13%), 1209 (21%) and 1080 (24%) observations.

C-N vibration: Considering the potential for band overlap in the vicinity, identifying the C-N stretching band is a challenging undertaking. The extension of CN vibrations in the 1350-1000 cm^{-1} range [35] will significantly help in the investigation of C-N vibrations through normal coordination assessment. Both theoretical and empirical calculations were conducted using FT-IR for the compound **4** at 1162(10%) and 1165 cm^{-1}, respectively.

FMO analysis: Fig. 5 shows an FMO diagram of compound **4** for gas phase. Positive and negative molecular orbital wavelengths are displayed in the red and green distributions [36]. In chemical processes, a smaller energy gap denotes greater reactivity. As shown in Table-3, the energy value of HOMO is -6.2216 eV and LUMO is -1.2449 eV and 4.9827eV is the orbital energy gap in compound **4**. These values correspond to bioactive compounds as they are below 5 eV [37]. Compounds having narrower band gaps interact more readily with reactants, hence enhancing their reactivity. The chemical hardness values of the compound **4** were determined to be 2.4914 (gas). Table-3 also shows the high hardness values of the title compound and its chemical stability.

TABLE-3
HOMO-LUMO ENERGY VALUE OF COMPOUND **4**, CALCULATED BY B3LYP METHOD WITH 6-311++G(d,p) BASIS SET

Molecular descriptors	Gas
HOMO (eV)	-6.2276
LUMO (eV)	-1.2449
Ionization potential	6.2276
Electron affinity	1.2449
Energy gap (eV)	4.9827
Electronegativity	3.7363
Chemical potential	-3.7363
Chemical hardness	2.4914
Chemical softness	0.2007
Electrophilicity index	2.8017

NBO-Fock matrix analysis: An analysis of natural bond orbitals was conducted to evaluate the stability of the chemical system concerning the charge delocalization from donor to acceptor level. The bond-antibonding interaction, which occurs when a donor orbital interacts with an acceptor orbital to exchange electrons, stabilizes the molecular structure [38]. NBO analysis employed a second-order Fock matrix to assess the donor-acceptor interactions [39]. The probe molecule is placed between the donor and acceptor states and energy calculations were performed. Table-4 summarizes the energy obtained from the perturbation.

$$E(2) = q_i \left(\frac{(F_{ij})^2}{(E_i - E_j)} \right)$$

where q_i = occupancy donor orbital, E(2) = stabilization energy, E_j, E_i and $F_{i,j}$ = diagonal/off-diagonal elements. The maximum stabilization energy of 206.48 kcal/mol is reported from the interaction σ*(C3-C4) to σ*(C5-C6), ranging from 17.6 to 21.4. In a similar manner, the electron delocalization energies of (7.89, 5.49, 5.1, 4.56, 4.36, 3.84, 2.79, 1.69, 1.45) are noted from the interaction ranging from σ(C14-C23) to σ*(C23-N24),

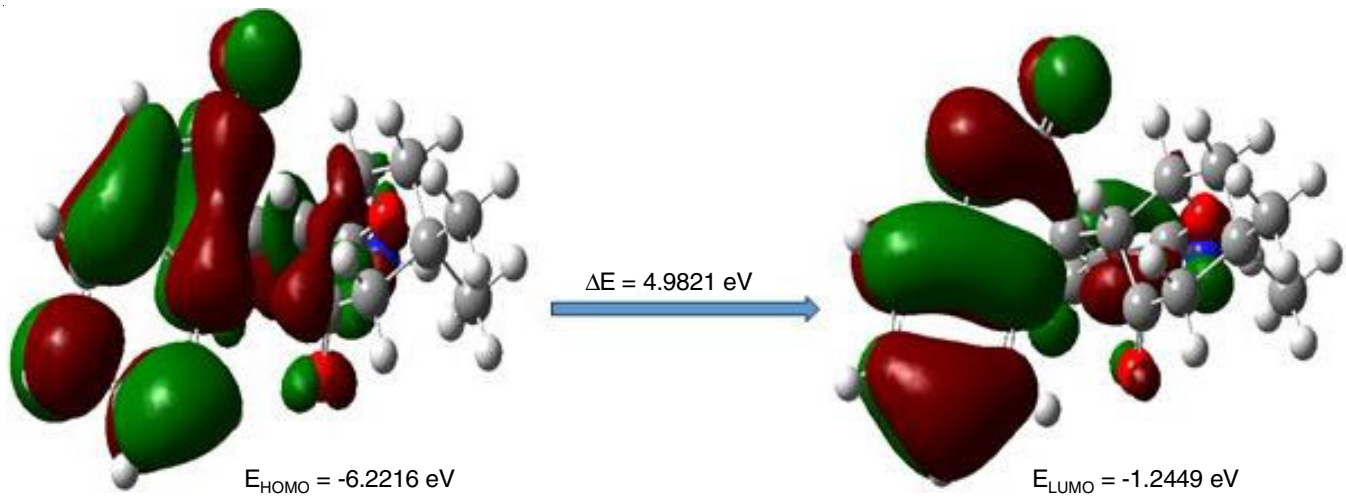

Fig. 5. Frontier molecular orbital (FMO) of compound **4**

TABLE-4
SECOND-ORDERS PERTURBATION THEORY ANALYSIS OF FOCK MATRIX IN NBO BASIS

Type	Donor (i)	Ed/e	Type	Acceptor (j)	Ed/e	E(2) (kcal/mol)	E(j)-E(i) (a.u.)	F(i,j) (a.u.)
σ	C1–C2	1.97931	σ*	C1–C6	0.01529	2.58	1.27	0.051
π	C1–C2	1.67872	π*	C3–C4	0.38751	17.6	0.27	0.063
σ	C1–C6	1.97602	σ*	C1–C2	0.0155	2.63	1.27	0.052
σ	C3–C4	1.97458	σ*	C2 – C3	0.01398	2.79	1.29	0.054
π	C3–C4	1.6691	π*	C1–C2	0.33111	21.4	0.3	0.071
σ	C3–H28	1.97935	σ*	C4–C5	0.02999	4.56	1.09	0.063
σ	C4–C5	1.96106	σ*	C3–C4	0.02197	5.1	1.27	0.072
π	C5–C6	1.67776	σ*	C9–C14	0.03701	2.29	0.66	0.038
σ	C6–H29	1.97752	σ*	C5–C6	0.02283	1.13	1.1	0.031
σ	C8–C9	1.95471	π*	C13–C14	0.35276	2.23	0.62	0.036
σ	C8–O19	1.99378	σ*	C4–N7	0.02749	1.09	1.5	0.036
σ	C9–C10	1.95079	σ*	C15–C16	0.05726	1.64	1	0.036
σ	C9–C14	1.94521	π*	C23–N24	0.01776	1.45	0.75	0.03
σ	C10–C11	1.95682	σ*	C5–C9	0.03454	2.51	1.04	0.046
σ	C10–C15	1.97317	σ*	C16–H33	0.01126	1.23	1.05	0.032
σ	C10–H31	1.95343	σ*	C9–C14	0.03701	2.7	0.93	0.045
σ	C11–O12	1.98373	σ*	C18–H35	0.01089	0.99	1.22	0.031
σ	C11–C18	1.97716	σ*	C9–C10	0.03308	1.92	0.99	0.039
σ	C11–H32	1.97355	σ*	C17–C18	0.03109	3.16	0.88	0.047
σ	O12–C13	1.98795	σ*	C11–C18	0.01816	0.88	1.31	0.03
σ	C14–C3	1.97294	σ*	C23–N24	0.01142	7.89	1.65	0.102
π	C15–O20	1.98272	σ*	C16–H34	0.01298	1.59	0.78	0.031
σ	C16–C17	1.95345	σ*	C22–H40	0.01126	1.69	1	0.037
σ	C16–H33	1.98026	σ*	C10–C15	0.07591	3.69	0.87	0.051
σ	C16–H34	1.96494	σ*	C17–C21	0.02361	3.33	0.88	0.049
σ	C18–H35	1.96883	σ*	C11–O12	0.04326	5.49	0.74	0.057
σ	C21–H37	1.98735	σ*	C16–C17	0.03058	3.78	0.85	0.051
σ	C21–H38	1.98777	σ*	C17–C22	0.01988	3.27	0.87	0.048
σ	C21–H39	1.98783	σ*	C17–C18	0.03109	3.84	0.86	0.052
σ	C22–H40	1.98717	σ*	C16–C17	0.03058	3.49	0.85	0.049
σ	N25–H43	1.98589	σ*	C13–C14	0.03131	4.22	1.26	0.065
σ	N25–H44	1.98383	σ*	O12–C13	0.0296	4.36	1.04	0.06
LP (1)	N7	1.65739	π*	C8–O9	0.27119	57.75	0.29	0.117
LP (1)	O12	1.95882	σ*	C10–C11	0.03368	2.2	0.91	0.04
LP (2)	O12	1.8365	π*	C13–C14	0.35276	33.09	0.36	0.103
LP (2)	O12	1.8365	σ*	C13–N25	0.02221	0.56	0.79	0.02
LP (2)	O19	1.84975	σ*	C11–H32	0.02844	1.14	0.69	0.026
LP (1)	O20	1.97411	σ*	C10–C15	0.07591	2.12	1.06	0.043
LP (2)	O20	1.8843	σ*	C15–C16	0.05726	19.74	0.66	0.103
LP (1)	N24	1.97036	σ*	C14–C23	0.02856	11.03	1.04	0.096
LP (1)	N25	1.78431	π*	C13–C14	0.35276	43.57	0.31	0.108
π*	C3–C4	0.38751	π*	C5–C6	0.32962	206.48	0.01	0.083

σ(C18-H35) to σ*(C11-O12), σ(C4-C5) to σ*(C3-C4), σ(C3-H28) to σ*(C4-C5), σ(C21-H39) to σ*(C17-C18), σ(C3-C4) to σ*(C2-C3), σ(C1-C2) to σ*(C1-C6), σ(C16-C17) to σ*(C22-H40) and σ(C9-C14) to σ*(C23-N24), respectively.

NMR studies: Using the GIAO approach with basis set, the predicted ^{13}C and ^{1}H chemical shift was calculated. The ^{13}C and ^{1}H theoretical and investigational spectra are displayed (Fig. 6a-b). The experimental and theoretic chemical changes are presented Table-5. Aromatic ring carbon chemical shift signals were found to range from 175 to 100 ppm [40,41].

The calculated chemical shift values from the DFT theoretical method align closely with the experimental findings. The carbon atoms connected to nitrogen and oxygen by double bonds were found to have a calculated chemical shift between 212.826 to 27.395 ppm, while the equivalent experimental shifts were found to be between 195.39 and 28.08 ppm. Protons on a methyl group carbon were predicted to have chemical shift values between 2 and 5 ppm. The aforementioned molecule contains 19 hydrogen bonds, NH and NH_2 groups. The observed chemical shift values for H29 to H39 in ^{1}H NMR ranged from 10.632 to 1.022 ppm, in contrast to the theoretical chemical shift values, which spanned from 8.356 to 0.725 ppm. The observed data and the anticipated chemical shift values align closely.

Molecular electrostatic potential (MEP): The nucleophilic and electrophilic reaction sites were investigated by using DFT technique in gas phase. The positive and negative potential

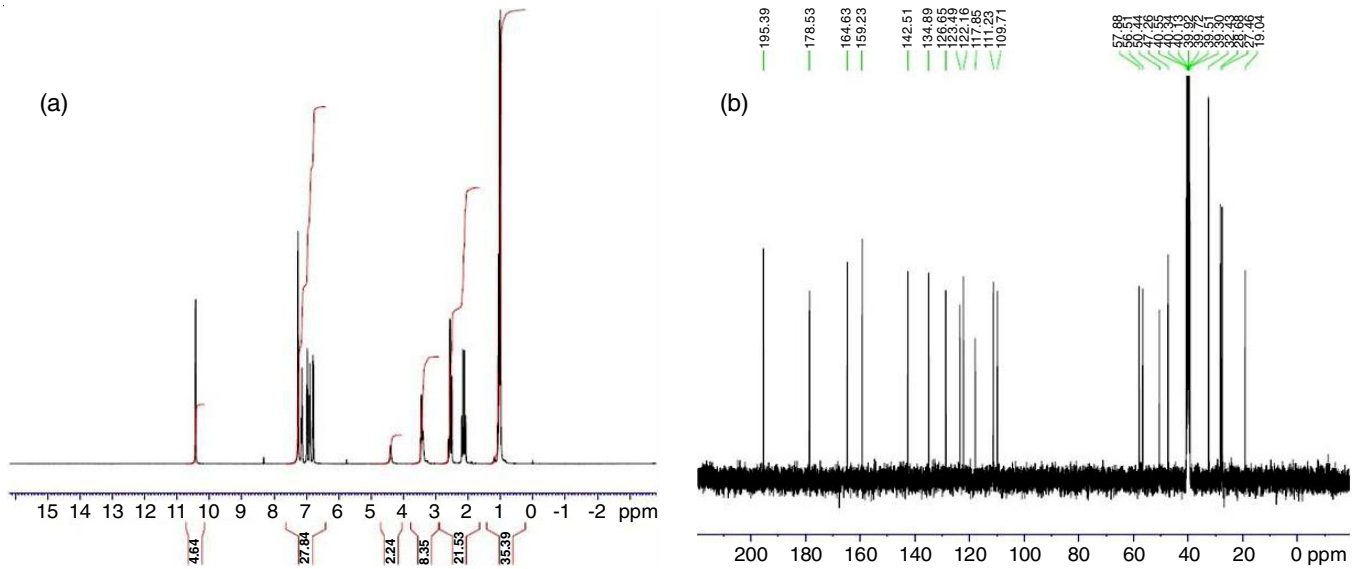

Fig. 6. (a) ^{1}H NMR and (b) ^{13}C NMR spectra for compound **4**

TABLE-5
OBSERVED AND PREDICTED ^{13}C AND ^{1}H NMR ISOTROPIC CHEMICAL SHIFTS FOR COMPOUND **4**

^{13}C NMR	Theoretical	Experimental	^{1}H NMR	Theoretical	Experimental
15-C	212.826	195.39	29-H	8.356	10.632
8-C	184.736	178.53	27-H	7.338	8.72
13-C	170.588	164.63	26-H	7.1	7.861
4-C	146.57	159.23	28-H	6.762	7.312
6-C	138.536	142.51	30-H	6.233	7.245
5-C	135.246	134.89	32-H	6.171	7.125
2-C	133.393	128.65	44-H	4.434	7.023
1-C	126.944	123.49	43-H	3.561	6.952
23-C	121.303	122.16	31-H	2.45	6.821
3-C	110.954	111.23	34-H	2.153	6.759
11-C	82.756	109.71	36-H	2.047	5.871
14-C	60.619	57.88	33-H	1.926	4.628
16-C	58.4	56.51	35-H	1.652	4.52
10-C	54.83	50.44	38-H	1.571	3.626
9-C	53.678	47.26	40-H	3.166	3.21
17-C	46.334	40.55	41-H	2.763	2.742
18-C	44.486	39.72	37-H	2.287	2.211
22-C	35.144	32.43	42-H	1.923	1.935
21-C	27.395	28.08	39-H	0.725	1.022

electrostatically of the study compound in gas around the atoms N24, C14 (-7.752 e^{-2}) to C3, C4 (+7.752 e^{-2}), respectively. The deepest blue (+ve) colour indicates nucleophilic area, red (-ve) colour indicates electrophilic area and possible natality denotes green colour. Fig. 7 shows a three-dimensional map of the MEP.

Fukui function analysis: Fukui functions, along with the examination of critical reactivity sites and comprehensive reactivity descriptions of molecules, provide the accurate prediction of atomic susceptibility to radical, nucleophilic and electrophilic attacks [42]. The Fukui function was frequently utilized to analyze the electrophilic and nucleophilic attacks. Dual-descriptor fr is the most suitable representation of reactive sites [43] and is represented as follows:

$$\Delta f(r) = f^{+}(r) - f^{-}(r)$$

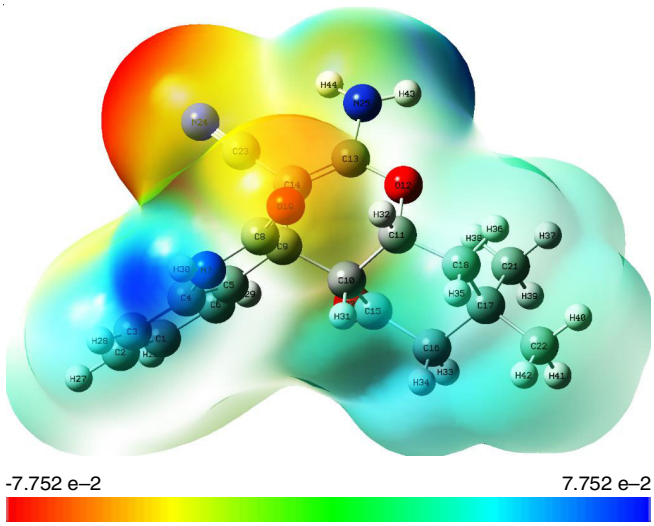

Fig. 7. MEP surface map of compound **4**

The electrophilic-nucleophilic compacted Fukui function (f0, f+r, f-r, f(r)) of compound **4** exhibits the highest efficacy, as illustrated in Table-6. Consequently, rather than utilizing MEP, it might be employed to ascertain the chemical locations. This can help determine if a molecule can provide or receive energy during a process. Based on Table-6, descriptor Δf(r) values, nucleophilic f+(r) sites are assumed to be like (C2 > C4 > C5 > N7 > C9 > C10 > C11 > O12 > C16 > O19 > C21 > 22 > 23 > N24 > N25 > H26). Electrophilic f-(r) are similarly as follows: C1 < C3 < C6 < C8 < C13 < C14 < C15 < C17 < O20 < H27 < H28 < H29 < H30 < H31 < H32 < H33 < H34 < H35 < H36 < H38 < H39 < H40 < H41 < H42 < H43 < H44.

Hyperpolarizability calculations: The first-order hyperpolarizability (β_{total}) and the related properties (μ, α and Δα) of compound **4** were examined using the finite-field method-based DFT/B3LYP approach. Hyperpolarizability is influenced by electron correlation and is highly sensitive to the theoretical level and basis sets utilized [44]. When compared to urea [45], compound **4** has higher values for total hyperpolarizability

TABLE-6
CONDENSED FUKUI FUNCTION AND DUAL DESCRIPTORS OF COMPOUND **4**

Atom	Mulliken atomic charges			Fukui functions			Dual descriptor Δf(r)	Local softness		
	0, 1 (N)	N + 1 (-1, 2)	N-1 (1,2)	f_r^+	f_r^-	f_r^0		sr + f_r^+	sr-f_r^-	sr0 f_r^0
1C	-0.288	-0.357	-0.261	-0.069	-0.028	-0.048	-0.041	-0.015	-0.006	-0.011
2C	-0.325	0.001	-0.302	0.326	-0.023	0.151	0.349	0.071	-0.005	0.033
3C	-0.486	-0.878	-0.444	-0.392	-0.042	-0.217	-0.351	-0.086	-0.009	-0.047
4C	-0.080	0.135	-0.063	0.215	-0.017	0.099	0.232	0.047	-0.004	0.022
5C	0.612	1.101	0.635	0.489	-0.023	0.233	0.512	0.107	-0.005	0.051
6C	-0.365	-0.540	-0.339	-0.175	-0.026	-0.101	-0.150	-0.038	-0.006	-0.022
7N	-0.250	-0.253	-0.211	-0.004	-0.039	-0.021	0.035	-0.001	-0.008	-0.005
8C	-0.134	-0.175	-0.110	-0.042	-0.024	-0.033	-0.018	-0.009	-0.005	-0.007
9C	1.417	1.814	1.228	0.398	0.188	0.293	0.209	0.087	0.041	0.064
10C	-0.257	0.108	-0.276	0.366	0.018	0.192	0.347	0.080	0.004	0.042
11C	-0.434	-0.195	-0.435	0.239	0.002	0.120	0.238	0.052	0.000	0.026
12O	0.004	0.043	0.059	0.040	-0.055	-0.008	0.094	0.009	-0.012	-0.002
13C	-0.193	-0.269	-0.133	-0.076	-0.060	-0.068	-0.017	-0.017	-0.013	-0.015
14C	1.117	0.972	1.225	-0.145	-0.108	-0.126	-0.037	-0.032	-0.023	-0.028
15C	-0.003	-0.479	0.034	-0.476	-0.037	-0.256	-0.439	-0.104	-0.008	-0.056
16C	-0.751	0.390	-0.780	1.142	0.029	0.585	1.112	0.249	0.006	0.128
17C	0.667	-0.953	0.557	-1.620	0.110	-0.755	-1.731	-0.353	0.024	-0.165
18C	-0.844	-0.031	-0.859	0.814	0.015	0.414	0.799	0.177	0.003	0.090
19O	-0.287	-0.294	-0.204	-0.007	-0.083	-0.045	0.075	-0.002	-0.018	-0.010
20O	-0.159	-0.234	-0.127	-0.074	-0.032	-0.053	-0.042	-0.016	-0.007	-0.012
21C	-0.600	-0.232	-0.568	0.368	-0.033	0.168	0.400	0.080	-0.007	0.037
22C	-0.467	0.555	-0.429	1.023	-0.038	0.492	1.061	0.223	-0.008	0.107
23C	-1.429	-1.086	-1.428	0.344	-0.002	0.171	0.345	0.075	0.000	0.037
24N	-0.205	-0.256	-0.074	-0.052	-0.131	-0.091	0.079	-0.011	-0.028	-0.020
25N	-0.300	-0.341	-0.204	-0.041	-0.096	-0.068	0.055	-0.009	-0.021	-0.015
26H	0.181	0.140	0.229	-0.041	-0.048	-0.044	0.007	-0.009	-0.010	-0.010
27H	0.162	0.100	0.211	-0.062	-0.049	-0.056	-0.013	-0.014	-0.011	-0.012
28H	0.155	-0.343	0.199	-0.498	-0.044	-0.271	-0.454	-0.108	-0.009	-0.059
29H	0.233	0.200	0.253	-0.033	-0.020	-0.027	-0.013	-0.007	-0.004	-0.006
30H	0.348	0.026	0.388	-0.323	-0.040	-0.181	-0.283	-0.070	-0.009	-0.039
31H	0.334	-0.228	0.366	-0.562	-0.032	-0.297	-0.530	-0.122	-0.007	-0.065
32H	0.320	0.137	0.336	-0.184	-0.015	-0.100	-0.168	-0.040	-0.003	-0.022
33H	0.232	0.166	0.258	-0.066	-0.026	-0.046	-0.039	-0.014	-0.006	-0.010
34H	0.158	-0.205	0.178	-0.363	-0.020	-0.192	-0.343	-0.079	-0.004	-0.042
35H	0.159	-0.092	0.183	-0.252	-0.024	-0.138	-0.228	-0.055	-0.005	-0.030
36H	0.219	0.101	0.241	-0.117	-0.023	-0.070	-0.095	-0.026	-0.005	-0.015
37H	0.158	0.013	0.179	-0.145	-0.021	-0.083	-0.124	-0.032	-0.004	-0.018
38H	0.212	0.232	0.187	0.020	0.025	0.022	-0.005	0.004	0.005	0.005
39H	0.150	0.019	0.173	-0.131	-0.023	-0.077	-0.108	-0.029	-0.005	-0.017
40H	0.151	0.032	0.167	-0.119	-0.016	-0.068	-0.103	-0.026	-0.004	-0.015
41H	0.154	-0.058	0.171	-0.213	-0.017	-0.115	-0.196	-0.046	-0.004	-0.025
42H	0.146	-0.245	0.157	-0.391	-0.011	-0.201	-0.381	-0.085	-0.002	-0.044
43H	0.269	0.191	0.311	-0.077	-0.043	-0.060	-0.035	-0.017	-0.009	-0.013
44H	0.298	0.267	0.323	-0.031	-0.025	-0.028	-0.006	-0.007	-0.005	-0.006

(1.29×10^{-30} e.s.u.) and polarizability (1.1405×10^{-23} e.s.u.) (Table-7).

Topology analysis: Depending on the covalent bond, the surface analysis yields maps of the localized orbital locator and electron localization function. The Multiwfn software suite was used to perform topological analysis [46,47]. A vibrant map that includes comprehensive details on localized orbital locator (LOL) and electron localization function (ELF) has been created and shown for compound **4** in Fig. 8(a,b) and (a1, b1), respect-ively. Colours ranging from blue to red indicate bonding and non-bonding electrons. The specified limit values for LOL and ELF are 0, 0.8 and 0.1 [48]. Electrons, whether bonding or non-bonding, are depicted as delocalized and localized electronic zones situated in the respective regions of (< 0.5 – > 0.5) [49]. The atoms of oxygen and hydrogen are indicated inside the red and blue areas.

RDG analysis: The investigation of chemical and organic systems is largely carried out by NCI. Red layers in the center of both the indoline and phenyl rings reveal an effect akin to the isosurface plot, while red peaks around 0.02 and 0.05 (au) suggest the steric influence. A mixed contour in blue-green among -0.03 and -0.02 a.u. illustrates the result of CHO attraction within the hydrogen bonding of the molecule. There appears to be significant hydrogen bonding [50]. The RDG figure illus-

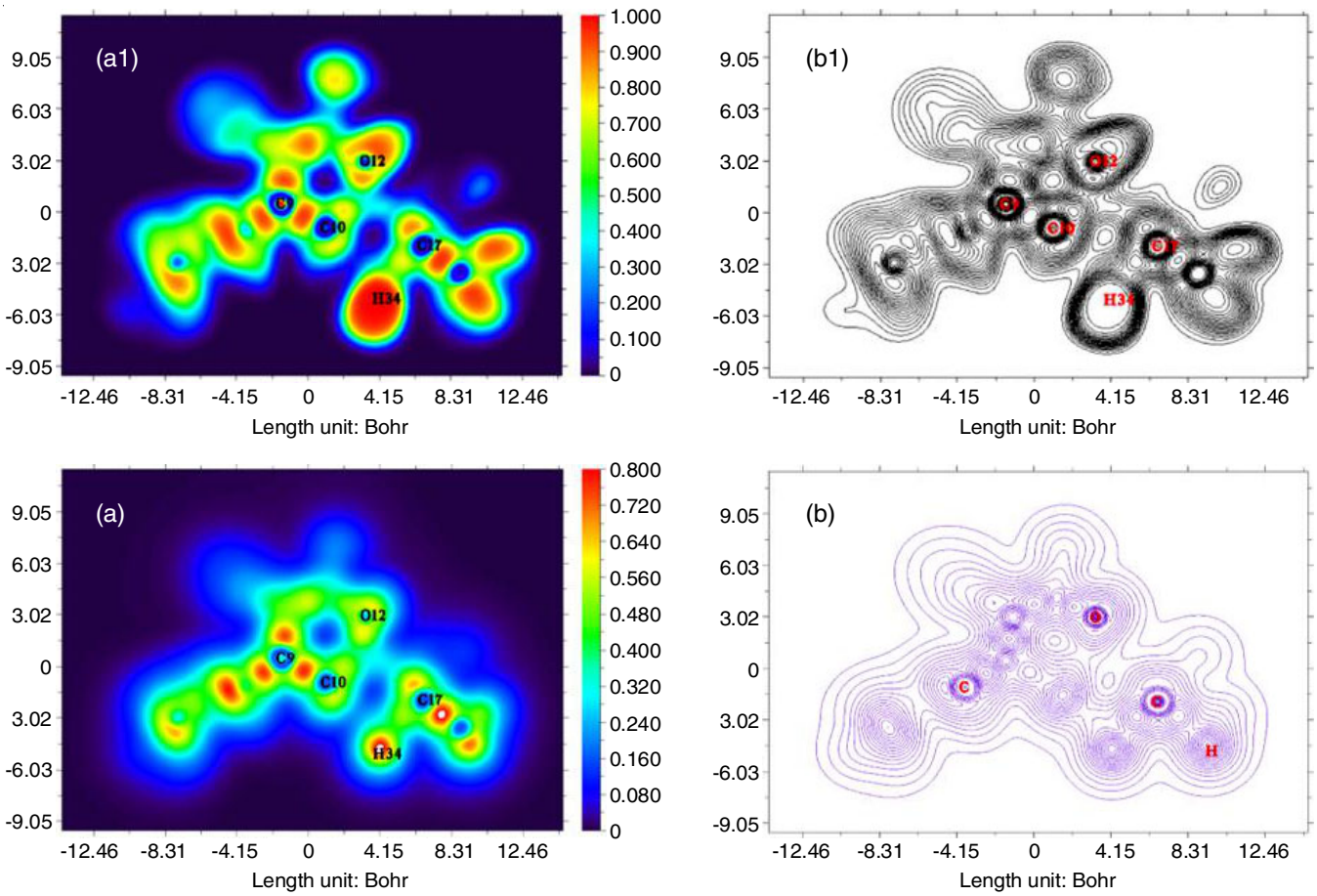

Fig. 8. Electron localization function (a,b), localized orbital locator (a1,b1) coloured diagram and contour maps of compound **4**

TABLE-7
CALCULATED DIPOLE MOMENT (D), POLARIZABILITY (α) AND FIRST ORDER HYPERPOLARIZABILITY (β) OF COMPOUND **4**

Parameter	B3LYP/ 6-311++G(d,p)	Parameter	B3LYP/ 6-311++G(d,p)
βxxx	-144.027	αxy	1.667
βxxy	6.135	αyy	226.804
βxyy	-111.876	αxz	-10.124
βyyy	-133.036	αyz	1.707
βzxx	-35.184	αzz	167.757
βxyz	18.346	α(a.u)	214.649
βzyy	7.726	α(e.s.u)	0.000
βxzz	-46.927	Δα (a.u)	438.071
βyzz	-49.182	Δα (e.s.u)	6.492×10^{-23}
βzzz	-65.568	μx	0.637
βtot (a.u)	362.444	μy	-0.128
βtot (e.s.u)	3.131×10^{-30}	μz	-0.094
αxx	249.387	μ(D)	0.657

trates that green sparkles between 0.01 and 0.00 a.u. represent small van der Waals forces between H-atoms. There is little variance in the results of the reduced density gradient between the media in this work. The 3D scatter and RDG graph are shown in Fig. 9.

Drug-likeness: To assess drug-likeness, several guidelines have been suggested. The most widely used and regarded as being very successful and efficient are the Veber rules [51], Lipinski's rule of five [52] and lipophilicity indices [53,54]. The results were assessed using the Swiss ADME web tool. Based on the standards, molecular mass < 500 Dalton, hydrogen bond donar less than (<)10, HBA < 5 and log P(<)5; orally active medications frequently only break the rules once. Table-8 illustrates that compound **4** is an excellent pharmaceutical alternative since it meets the Lipinski requirements, making it a perfect candidate for medicine that does not violate the Lipinski rules.

***In vitro* analysis:** NCI-USA investigated the anticancer activity of synthesized spirooxindole-chromene derivative with 60 human cancer cell lines at an amount of 10^{-5} molar and generated an NSC code (Table-9) that could be used for retrieving anticancer activity from the NCI database. However, only one dosage screening results were supplied, which demonstrated suppression of cancer cells by synthesized compound **4**. As a result, in the leukemia panel, compound **4** demonstrated the highest percentage growth inhibition, 5.39, against the K-562 cancer cell line. Moreover, in the panel for non-small lung cancer, the synthesized compound did not inhibit any cancer cell lines. Despite one cancer cell, namely HCC-2998, being inhibited by a compound of approximately 6.66% GI, other cancer cell lines were not inhibited under the colon cancer panel. The synthesized compound **4** showed the highest growth inhibition for only two cell lines, namely, SF-539 and SNB-19

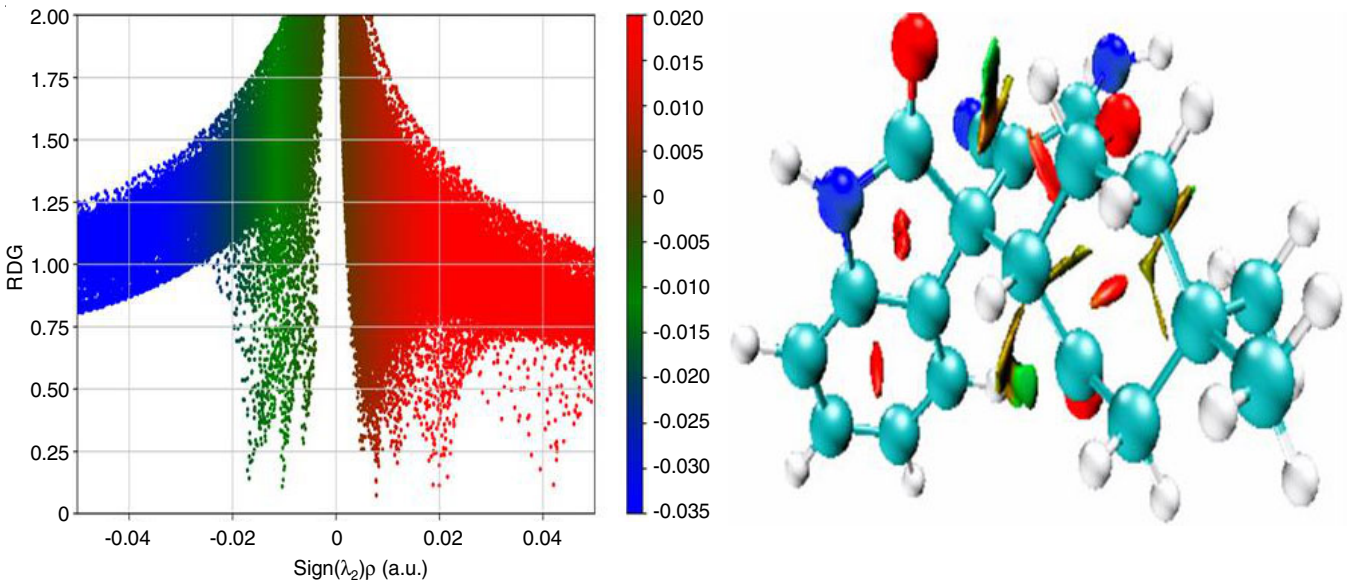

Fig. 9. Reduced density gradient (RDG) colour-filled map of compound **4**

TABLE-8
DRUG-LIKENESS OF COMPOUND **4**

Lipinski rules				Veber's rules	
Molecular weight (g/mol)	MLog P	Hydrogen bond donors	Hydrogen bond acceptors	Topological polar surface area (Å^2)	Number of rotatable bonds
337.37	0.87	4	2	105.21	1

TABLE-9
ONE DOSE MEAN GRAPH OF SIXTY HUMAN CANCER CELL LINES

Panel name/ NSC: 845946	Cell number	Cell name	Growth (%)	Panel name/ NSC: 845946	Cell number	Cell name	Growth (%)
Leukemia	3	CCRF-CEM	108.2837	Melanoma	14	M14	101.8057
Leukemia	8	HL-60(TB)	100.7105	Melanoma	11	MDA-MB-435	106.5682
Leukemia	5	K-562	94.61362	Melanoma	5	SK-MEL-2	107.3659
Leukemia	6	MOLT-4	117.1667	Melanoma	8	SK-MEL-28	103.4091
Leukemia	10	RPMI-8226	104.158	Melanoma	7	SK-MEL-5	101.4133
Non-small cell lung cancer	4	A549/ATCC	107.1085	Melanoma	21	UACC-257	97.42527
Non-small cell lung cancer	8	EKVX	103.9261	Ovarian cancer	10	IGROV1	118.0765
Non-small cell lung cancer	26	HOP-62	104.5959	Ovarian cancer	1	OVCAR-3	106.6047
Non-small cell lung cancer	29	HOP-92	107.7387	Ovarian cancer	2	OVCAR-4	120.103
Non-small cell lung cancer	13	NCI-H226	107.882	Ovarian cancer	3	OVCAR-5	101.1501
Non-small cell lung cancer	1	NCI-H23	101.2373	Ovarian cancer	5	OVCAR-8	100.3569
Non-small cell lung cancer	17	NCI-H322M	114.6335	Ovarian cancer	2	NCI/ADR-RES	101.5337
Non-small cell lung cancer	21	NCI-H460	125.2065	Ovarian cancer	11	SK-OV-3	116.0173
Non-small cell lung cancer	3	NCI-H522	102.8722	Renal cancer	18	786-0	107.9409
Colon cancer	10	COLO 205	117.9067	Renal cancer	13	A498	133.0598
Colon cancer	2	HCC-2998	93.34853	Renal cancer	23	ACHN	100.7466
Colon cancer	3	HCT-116	104.7292	Renal cancer	15	CAKI-1	104.5128
Colon cancer	15	HCT-15	107.2798	Renal cancer	16	RXF 393	113.0728
Colon cancer	1	HT29	107.6388	Renal cancer	8	SN12C	104.3424
Colon cancer	17	KM12	108.3473	Renal cancer	24	TK-10	100.5836
Colon cancer	9	SW-620	124.2942	Renal cancer	4	UO-31	82.12542
Cns cancer	14	SF-268	103.3511	Prostate cancer	1	PC-3	98.33278
Cns cancer	15	SF-295	104.2458	Prostate cancer	3	DU-145	110.2133
Cns cancer	16	SF-539	97.57209	Breast cancer	1	MCF7	92.2482
Cns cancer	2	SNB-19	96.856	Breast cancer	5	MDA-MB-231/ATCC	115.1212
Cns cancer	5	SNB-75	116.9159	Breast cancer	6	HS 578T	116.7887
Cns cancer	9	U251	101.4766	Breast cancer	13	BT-549	178.0037
Melanoma	1	LOX IMVI	100.1969	Breast cancer	18	MDA-MB-468	106.786
Melanoma	2	MALME-3M	118.7236				

cancer cell lines, *i.e.*, 2.43 and 3.15% GI, respectively. The remaining cells did not show inhibition under the CNS cancer panel. Of all melanoma cancer cells, only one, namely, UACC-257, showed a 2.58% GI against compound **4** and the remaining cells did not inhibit. Similarly, compound **4** showed 17.88% growth inhibition against only the single renal cancer UO-31 cell line, others did not inhibit. Next is the prostate cancer cell panel, herein, compound **4** showed 1.67% GI against the PC-3 cell line. In line with the developing treatment program, breast cancer is the last panel and synthesized compound **4** was found to be an anti-breast agent for the MCF-7 cell line at 7.76% GI. Therefore, this compound **4** could be derivatized in the future through chemical reactions to make more potent anti-renal cancer drugs owing to it showing the highest cell growth inhibition.

Molecular docking: To perform the molecular docking analyses, the AutoDock 4.2.1 Tools software was used. PyMOL [55] was used for target protein preparation when the target proteins are identified *via* the PASS online service [56]. Using BIOVIA's Discovery Studio Visualiser, the visualized complex is obtained after the docking process, allowing for the extraction of important interactions within the complex. The proteins were chosen from the RCSB database [57]. Figs. 10 and 11 show the interactions between the protein and ligand with different target protein residues. Table-10 displays the ligand-receptors used in this investigation along with their binding affinity values.

The structure of the target proteins (PDB IDs: 4DRI, 8BR9 and 6CZ4) can be obtained by utilizing Protein Data Bank. The maximal binding affinity (-7.76 kcal/mol) of the chemical with the title has numerous relationships (PDB-4DRI). For this molecule, there were 5 typical hydrogen bonds found at protein residues at GLN156, ASN199, GLU195 and ASP192. Two alkyl groups (ARG230, LEU191) have been shown to interact with this compound at 2.31, 2.65, 1.97, 2.34, 2.22, 3.39 and 4.35 Å,

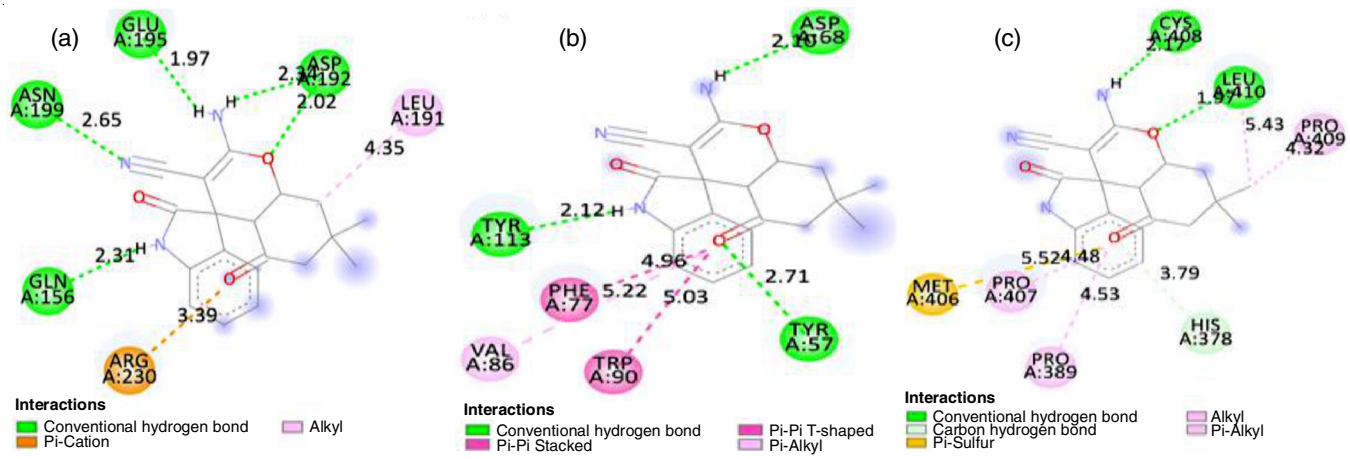

Fig. 10. Compound **4** (2D) and targeted proteins (8BR9, 4DRI and 6CZ4)

TABLE-10
MOLECULAR DOCKING CHARACTERISTIC OF COMPOUND **4** WITH TARGETED PROTEINS

Protein	Ligand	Binding energy (kcal/mol)	Ligand groups	Protein residues	*Type of interaction	Bond distance (Å)
4DRI	Compound **4**	-7.76	CO	TYR113	Conventional hydrogen bond	2.71
			NH	ASP68	Conventional hydrogen bond	2.12
			CH_{ring}	TYR57	Conventional hydrogen bond	2.09
			CH_{ring}	PHE77	Pi-Pi Stacked/shaped	4.96
			CH_{ring}	TRP90	Pi-Pi Stacked/shaped	5.23
			CH_{ring}	TRP90	Pi-Pi T-shapped	4.91
			CH_{ring}	VAL86	Pi-Alkyl	5.21
6CZ4		-7.3	NH	CYS408	Conventional hydrogen bond	2.17
			CO	LEU410	Conventional hydrogen bond	1.97
			NH	PRO409	Pi-Alkyl	4.32
			CH_{ring}	HIS 378	Carbon hydrogen bond	3.79
			CH_{ring}	PRO389	Alkyl	4.53
			CH_{ring}	PRO407	Pi-Alkyl	4.48
			CH_{ring}	MET406	Pi-Sulfur	5.52
8BR9		-6.59	CO	GLN156	Conventional hydrogen bond	2.01
			NH	ASN199	Conventional hydrogen bond	2.65
			CN	GLU195	Conventional hydrogen bond	2.3
			OH	ASP192	Conventional hydrogen bond	2.34
			CH_{ring}	ARG230	Pi-Cation	3.38
			CH_{ring}	LEU191	Alkyl	4.43

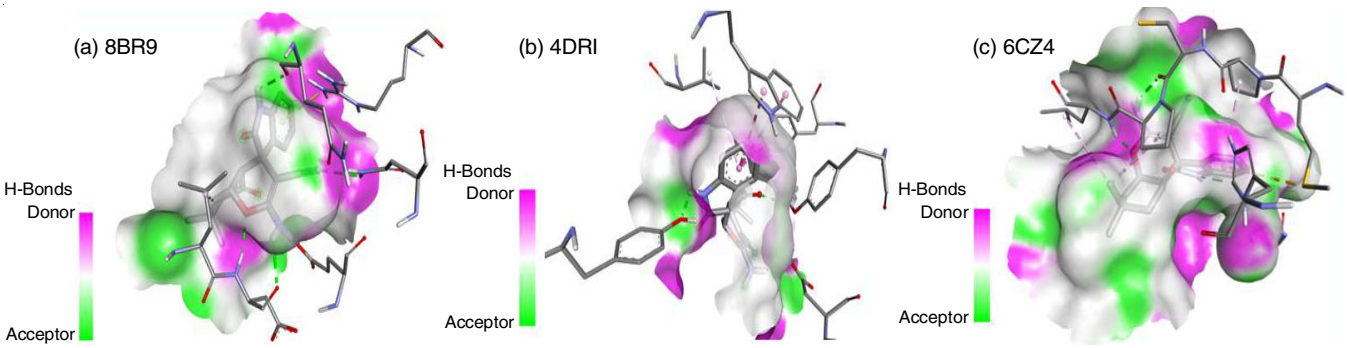

Fig. 11. Compound **4** docked into binding site (3D) of an anti-breast cancer proteins (8BR9, 4DRI and 6CZ4)

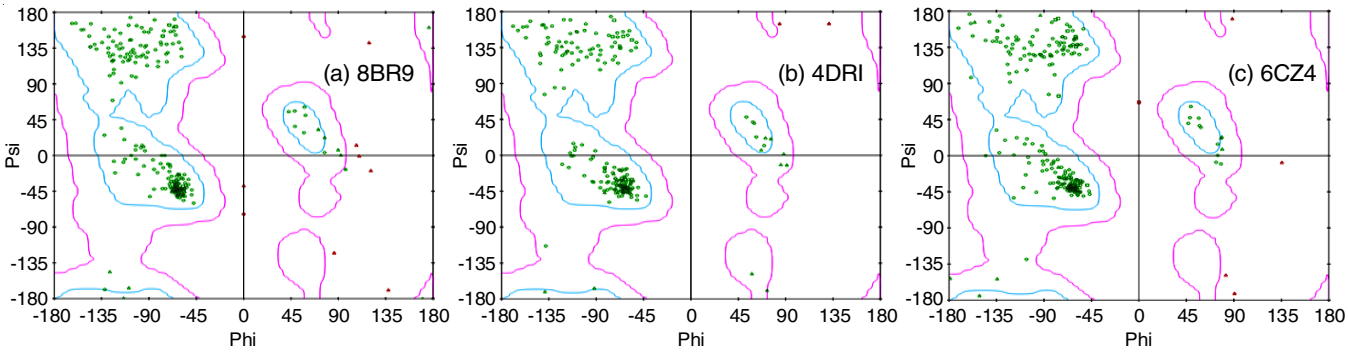

Fig. 12. Ramachandran plot for target proteins

respectively. The results obtained demonstrate the molecule's powerful anti-breast cancer disease activity. Fig. 12 presents Ramachandran plots for the three proteins, illustrating the energetically permissible regions based on the ψ and ϕ values of the amino acid residues in a selected protein structure. The conformational zones or regions permitted to execute docking in high binding mode, are indicated by blue areas in Ramachandran plots. In light of these findings, compound **4** may play a key role in medicinal chemistry by demonstrating potential anti-breast cancer activity following permitted areas and binding interactions.

Conclusion

A novel spirooxindole-chromene compound (**4**) was carried out with Et_3N as catalyst which underwent Knoevenegel and Michael addition reactions. The molecular structures of the compound **4** were optimized using the DFT/B3LYP method and 6-311G(d,p) basis set. The bond length and bond angle of optimized molecular features have been found using a high-level basis set. Potential energy distribution data and comprehensive FT-IR and FT-Raman spectra have been applied to identify vibrational modes.It was found that the FMO energy gap of compound **4** indicated it was a flexible molecule capable of readily binding to biomolecules and initiating biological processes. When experimental and computed NMR chemical shift parameters were compared, both ^{1}H and ^{13}C NMR showed a excellent correlation. All of the atomic sites were analyzed for reactive sites on reference chemical surfaces using MESP and the Fukui function. The peculiarities of surface forecasts influenced by covalent connections are elucidated by topological studies utilizing the Multiwave function. Moreover, weak and steric repulsive regions as well as strong hydrogen bonds were identified using the RDG analysis scatter graph. The effectiveness of compound **4** as an NLO material is demonstrated by nonlinear optical investigations. NBO analysis explains inter and intramolecular interactions. The docking and drug-likeness studies confirm the anti-breast cancer therapeutic potential of compound **4**, despite its lower binding affinity of -6.59 kcal/mol. *In vitro* experiments validate that the synthesized compound **4** was found to be 7.76% GI anti-breast agent for the MCF-7 cell line.

CONFLICT OF INTEREST

The authors declare that there is no conflict of interests regarding the publication of this article.

REFERENCES

1. S.M. Umer, M. Solangi, K.M. Khan and R.S.Z. Saleem, *Molecules,* **27**, 7586 (2022); https://doi.org/10.3390/molecules27217586
2. U. Anand, A. Dey, A.K. Singh Chandel, R. Sanyal, A. Mishra, D.K. Pandey, V. De Falco, A. Upadhyay, R. Kandimalla, A. Chaudhary, J.K. Dhanjal, S. Dewanjee, J. Vallamkondu and J.M.P. de la Lastra, *Genes Dis.*, **10**, 1367 (2022); https://doi.org/10.1016/j.gendis.2022.02.007
3. L.M. Zhou, R.Y. Qu and G.F. Yang, *Expert Opin. Drug Discov.*, **15**, 603 (2020); https://doi.org/10.1080/17460441.2020.1733526
4. H. Hong, L.J. Huang and D.W. Teng, *Chinese Chem. Lett.*, **22**, 1009 (2011); https://doi.org/10.1016/j.cclet.2011.01.042
5. M. Kaur, B. Singh, B. Singh and A. Arjuna, *J. Heterocycl. Chem.*, **54**, 1348 (2017); https://doi.org/10.1002/jhet.2712

6. S.T. Al-Rashood, A.R. Hamed, G.S. Hassan, H.M. Alkahtani, A.A. Almehizia, A. Alharbi, M.M. Al-Sanea and W.M. Eldehna, *J. Enzyme Inhib. Med. Chem.*, **35**, 831 (2020); https://doi.org/10.1080/14756366.2020.1743281
7. M. Asif, F. Aqil, F.A. Alasmary, A. almalki, A.R. Khan and M. Nasibullah, *Med. Chem. Res.*, **32**, 1001 (2023); https://doi.org/10.1007/s00044-023-03053-7
8. M. Asif, S.S. Alvi, T. Azaz, A.R. Khan, B. Tiwari, B.B. Hafeez and M. Nasibullah, *Int. J. Mol. Sci.*, **24**, 7336 (2023); https://doi.org/10.3390/ijms24087336
9. M. Asif, M. Saquib, A.R. Khan, F. Aqil, A.S. Almalki, F.A. Alasmary, J. Singh and M. Nasibullah, *ChemistrySelect*, **8**, e202204536 (2023); https://doi.org/10.1002/slct.202204536
10. M. Asif, R. Srivastava, A. Fatima, M. Shakeel, F. Hassan and M. Nasibullah, *Russ. J. Bioorg. Chem.*, **49**, 1165 (2023); https://doi.org/10.1134/S1068162023060018
11. M. Asif, T. Azaz, B. Tiwari and M. Nasibullah, *Tetrahedron*, **134**, 133308 (2023); https://doi.org/10.1016/j.tet.2023.133308
12. D. Kumar, P. Sharma, H. Singh, K. Nepali, G.K. Gupta, S.K. Jain and F. Ntie-Kang, *RSC Adv.*, **7**, 36977 (2017); https://doi.org/10.1039/C7RA05441F
13. V. Raj and J. Lee, *Front. Chem.*, **8**, 623 (2020); https://doi.org/10.3389/fchem.2020.00623
14. U. Agarwal, R.K. Tonk and S. Paliwal, *Curr. Drug Discov. Technol.*, **22**, e15701638361318 (2025); https://doi.org/10.2174/0115701638361318241230073123
15. R.B.O. Ouma, S.M. Ngari and J.K. Kibet, *Discov. Public Health*, **21**, 108 (2024); https://doi.org/10.1186/s12982-024-00229-3
16. F. Jabeen, Q.I. Rahman and S. Zafar, *Int. J. Appl. Chem.*, **6**, 18 (2019); https://doi.org/10.14445/23939133/IJAC-V6I3P104
17. M.J. Frisch, G.W. Trucks, H.B. Schlegel, G.E. Scuseria, M.A. Robb and J.R. Cheeseman, Gaussian 16, Gaussian Inc, Walling-form CT (2010).
18. R. Dennington, T.A. Keith and J.M. Millam, GaussView, Version 6, Semichem Inc., Shawnee Mission, KS (2016).
19. G.A. Zhurko and D.A. Zhurko, Chemcraft. Version 1.7 (Build 132), (2014).
20. J.P. Merrick, D. Moran and L. Radom, *J. Phys. Chem. A*, **111**, 11683 (2007); https://doi.org/10.1021/jp073974n
21. H. Jamroz, *Spectrochim. Acta A Mol. Biomol. Spectrosc.*, **114**, 220 (2013); https://doi.org/10.1016/j.saa.2013.05.096
22. L. Tian and F. Chen, *J. Comput. Chem.*, **33**, 466 (2012); https://doi.org/10.1002/jcc.21992
23. S. Armakovic and S.J. Armakovic, *Mol. Simul.*, **49**, 117 (2023); https://doi.org/10.1080/08927022.2022.2126865
24. S. Armakovic and S.J. Armakovic, *Mol. Simul.*, **50**, 560 (2024); https://doi.org/10.1080/08927022.2024.2329736
25. A. Daina, O. Michielin and V. Zoete, *Sci. Rep.*, **7**, 42717 (2017); https://doi.org/10.1038/srep42717
26. G.M. Morris, R. Huey, W. Lindstrom, M.F. Sanner, R.K. Belew, D.S. Goodsell and A.J. Olson, *J. Comput. Chem.*, **30**, 2785 (2009); https://doi.org/10.1002/jcc.21256
27. D.S. Biovia, Discovery Studio Modeling environment, Release 4.5, 4, Dassault Systemes BIOVIA, San Diego (2015).
28. S.C. Parakkal, R. Datta, S. Muthu, A. Irfan and A. Jeelani, *J. Mol. Liq.*, **359**, 119234 (2022); https://doi.org/10.1016/j.molliq.2022.119234
29. B. Fathima Rizwana, J.C. Prasana, S. Muthu and C.S. Abraham, *J. Mol. Struct.*, **1202**, 127274 (2020); https://doi.org/10.1016/j.molstruc.2019.127274
30. B. Amul, S. Muthu, M. Raja and S. Sevvanthi, *J. Mol. Struct.*, **1210**, 128040 (2020); https://doi.org/10.1016/j.molstruc.2020.128040
31. F. Basha A, F.L.A. Khan, S. Muthu and M. Raja, *Chem. Data Coll.*, **31**, 100609 (2021); https://doi.org/10.1016/j.cdc.2020.100609
32. A. Jeelani, S. Muthu, P. Ramesh and A. Irfan, *J. Mol. Liq.*, **358**, 119166 (2022); https://doi.org/10.1016/j.molliq.2022.119166
33. J.D. Magdaline and T. Chithambarathanu, *Mater. Today Proc.*, **2**, 982 (2015); https://doi.org/10.1016/j.matpr.2015.06.021
34. S.M. Hiremath, A. Suvitha, C.S. Hiremath, S.S. Khemalapure, S.K. Pattanayak, N.R. Patil, V.S. Negalurmath and K. Obelannavar, *J. Mol. Struct.*, **1171**, 362 (2018); https://doi.org/10.1016/j.molstruc.2018.05.109
35. K.R. Jennings, *Org. Mass Spectrom.*, **26**, 813 (1991); https://doi.org/10.1002/oms.1210260923
36. R.A. Shinde, V.A. Adole, R.S. Shinde, B.S. Desale and B.S. Jagdale, *Results Chem.*, **4**, 100553 (2022); https://doi.org/10.1016/j.rechem.2022.100553
37. A. Herlin Shamina, V. Bena Jothy, M. Asif, M. Nasibullah, N.S. Alharbi, G. Abbas and S. Muthu, *J. Mol. Liq.*, **391**, 123288 (2023); https://doi.org/10.1016/j.molliq.2023.123288
38. A.E. Reed and F. Weinhold, *J. Chem. Phys.*, **78**, 4066 (1983); https://doi.org/10.1063/1.445134
39. E. Scrocco and J. Tomasi, Advances in Quantum Chemistry, Academic Press: New York (1978).
40. C. Alasalvar, N. Öztürk, A.A.M. Abdel-Aziz, H. Gökce, A.S. El-Azab, M.A. El-Gendy and Y. Sert, *J. Mol. Struct.*, **1171**, 696 (2018); https://doi.org/10.1016/j.molstruc.2018.06.038
41. L.M. Amzel, D.F. Covey, C. Fenselau, A. Nickon and C.H. Robinson, *Biol. Mass Spectrom.*, **4**, vii (1977); https://doi.org/10.1002/bms.1200040612
42. R.I. Al-Wabli, K.S. Resmi, Y.S. Mary, C.Y. Panicker, M.I. Attia, A.A. El-Emam and C. Van Alsenoy, *J. Mol. Struct.*, **1123**, 375 (2016c); https://doi.org/10.1016/j.molstruc.2016.07.044
43. C. Morell, A. Grand and A. Toro-Labbé, *J. Phys. Chem. A*, **109**, 205 (2005); https://doi.org/10.1021/jp046577a
44. G. Velraj, S. Soundharam and C. Sridevi, *J. Mol. Struct.*, **1060**, 156 (2014); https://doi.org/10.1016/j.molstruc.2013.12.040
45. M. Maria Julie, T. Prabhu, E. Elamuruguporchelvi, F.B. Asif, S. Muthu and A. Irfan, *J. Mol. Liq.*, **336**, 116335 (2021); https://doi.org/10.1016/j.molliq.2021.116335
46. B. Silvi and A. Savin, *Nature*, **371**, 683 (1994); https://doi.org/10.1038/371683a0
47. F.R. B, J.C. Prasana, S. Muthu and C.S. Abraham, *Comput. Biol. Chem.*, **78**, 9 (2019); https://doi.org/10.1016/j.compbiolchem.2018.11.014
48. T.K. Kuruvilla, S. Muthu, J.C. Prasana, J. George and S. Sevvanthi, *J. Mol. Struct.*, **1175**, 163 (2019); https://doi.org/10.1016/j.molstruc.2018.07.097
49. B.F. Rizwana, J.C. Prasana, S. Muthu and C.S. Abraham, *Mater. Today Proc.*, **18**, 1770 (2019); https://doi.org/10.1016/j.matpr.2019.05.276
50. N.K. Nkungli and J.N. Ghogomu, *J. Mol. Model.*, **23**, 200 (2017); https://doi.org/10.1007/s00894-017-3370-4
51. D.F. Veber, S.R. Johnson, H.Y. Cheng, B.R. Smith, K.W. Ward and K.D. Kopple, *J. Med. Chem.*, **45**, 2615 (2002); https://doi.org/10.1021/jm020017n
52. C.A. Lipinski, F. Lombardo, B.W. Dominy and P.J. Feeney, *Adv. Drug Deliv. Rev.*, **23**, 3 (1997); https://doi.org/10.1016/S0169-409X(96)00423-1
53. A.L. Hopkins, G.M. Keserü, P.D. Leeson, D.C. Rees and C.H. Reynolds, *Nat. Rev. Drug Discov.*, **13**, 105 (2014); https://doi.org/10.1038/nrd4163
54. P.D. Leeson and B. Springthorpe, *Nat. Rev. Drug Discov.*, **6**, 881 (2007); https://doi.org/10.1038/nrd2445
55. The PyMOL Molecular Graphics System, Version 1.8 Schrodinger, LLC (2015).
56. D.A. Filimonov, A.A. Lagunin, T.A. Gloriozova, A.V. Rudik, D.S. Druzhilovskii, P.V. Pogodin and V.V. Poroikov, *Chem. Heterocycl. Compd.*, **50**, 444 (2014); https://doi.org/10.1007/s10593-014-1496-1
57. H.M. Berman, T. Battistuz, T.N. Bhat, W.F. Bluhm, P.E. Bourne, K. Burkhardt, Z. Feng, G.L. Gilliland, L. Iype, S. Jain, P. Fagan, J. Marvin, D. Padilla, V. Ravichandran, B. Schneider, N. Thanki, H. Weissig, J.D. Westbrook and C. Zardecki, *Acta Crystallogr.*, **58**, 899 (2002); https://doi.org/10.1107/s0907444902003451